Synthesis and characterisation of cobalt hydroxy carbonate $Co_2CO_3(OH)_2$ Nanomaterials

Jing (Jeanne) Yang and Ray L. Frost •

Inorganic Materials Research Program, School of Physical and Chemical Sciences, Queensland University of Technology, GPO Box 2434, Brisbane Queensland 4001, Australia.

Abstract:

In an attempt to make nanofibres based upon cobalt oxides, a novel compound a hydrated cobalt hydroxy carbonate was formed. This compound is related to the minerals of the rosasite mineral group. X-ray diffraction showed that the formed compound was a cobalt hydroxy carbonate and SEM displayed bundles of fibres on the micron scale in length and nanoscale in width. The morphology was compared with that of the rosasite mineral group. XPS proved two bond energies for cobalt and three for oxygen in the compound. The compound was characterised by vibrational spectroscopy and the spectra related to minerals of the rosasite mineral group. The stability of the synthetic mineral was limited to temperatures below 200°C.

Keywords: XRD, Raman, Infrared, SEM, cobalt hydroxide, cobalt oxide, cobalt carbonate

• Author to whom correspondence should be addressed (r.frost@qut.edu.au)

Introduction

In recent years, synthesis of inorganic nanoscale materials with special morphologies has been of great interest in material science [1, 2], because their intrinsic properties nanoscale materials are mainly determined by their composition, structure, crystallinity, size and morphology [3]. In particular, one dimensional (1D) nanoscale inorganic materials including nanofibers, nanowires and nanotubes have attracted intensive interest due to their distinctive geometries, novel physical and chemical properties and potential applications in numerous areas [4]. Because of its high surface area, chemical and thermally stable properties and mesoporous properties, metal oxides have been extensively used as carrier and support for a variety of industrial catalysts at high temperature as well as low temperature. The oxides of cobalt can be employed as catalyst [5], adsorbent [6, 7], composite materials [8, 9] and ceramics [10-12].

Transition metal oxides are widely used in the field of heterogeneous catalysis. Cobalt oxide and its derived compounds have are especially interesting due to their exceptional physical and chemical properties, which make them promising materials widely applied in rechargeable Li-ion batteries [13, 14], gas sensing [15], catalysis [16, 17], ionic exchangers [18], and magnetic materials[19], et al. Cobalt oxide (Co_3O_4) is an important magnetic p-type semiconductor with an indirect bandgap of 1.5 eV [20]. Li et al. [21] reported in 2005 that Co_3O_4 nanotubes, nanorods, and nanoparticles can be used as the anode materials of lithium-ion batteries. Especially the Co_3O_4 nanotubes prepared with template displayed high discharge capacity and superior cycling reversibility and excellent sensitivity to hydrogen and alcohol. Cobalt oxyhydroxide (CoOOH) is considered as a nonstoichiometric oxyhydroxide and has more oxidation state (Co^{3+}) than Co_3O_4. In recent years, CoOOH has been applied as an alternative material for CO detection, to improve a Co_3O_4-based gas sensor. Geng et al [22] synthesized the hierarchical dumbbell like CoOOH nanostructures, which have large active surface area and exhibited a superior sensitivity to CO at room temperature, as well as good reproducibility and short response/recovery time. These as-prepared CoOOH nanostructures could be potential nanosensors.

It is well known that intrinsic properties of inorganic materials are mainly determined by their composition, structure, crystallinity, size and morphology; great efforts have been devoted to investigation of different cobalt oxyhydroxide and cobalt oxides materials synthesis. It is reported that after 4 hour-calcination at 400 ºC, one dimensional hierarchical Co_3O_4 nanocolumns were obtained from $Co(OH)_2$ prepared through one-step hydrothermal synthesis with hydrazine hydrate and Na_3PO_4 as morphology directing agents [23]. Yang et al [24] successfully synthesized CoOOH hierarchically hollow spheres by nanorods self-assembly through bubble templating. Cobalt oxides with novel structure can be controlled synthesised from suitable precursors. The present of carbonate in the synthesis process of cobalt hydroxide precursors can result unique morphology of the products. 3D sisal-like, dandelion-like and rose-like architectures of cobalt hydroxide carbonate were synthesised through a selected-control hydrothermal process [25]. As a precursor of Co_3O_4 nanorods for CO oxidation catalyst, nanorod-shaped cobalt hydroxide carbonate was obtained by the precipitation of cobalt acetate with sodium carbonate incorporating ethylene glycol [17]. Xu and Zeng [26] reported a detailed investigation on formation of cobalt basic carbonate compounds with dimensional and morphological controls. In this work, cobalt hydroxide carbonate with fibrous morphology was synthesized in the assistance of urea and Na_3PO_4.

The oxides of cobalt are also a crucial precursor in sol-gel technique for preparing high-purity and high-strength monolithic cobalt oxide ceramics for use as substrates for electronic circuits, abrasive grains, high-temperature refractory materials, fibres and thin films [27]. Since the resulting cobalt oxide prepared from a number of common chemicals can keep the original size and morphology after calcination, great effort has been devoted to the investigation of nanoscale materials, especially 1D nanostructures, such as nanofibres and nanotubes [28, 29]. In this work, attempts were made at synthesising nanofibres based upon the compounds of cobalt including cobalt oxides and cobalt carbonate. In this paper we report the synthesis and characterisation of nanofibers based upon cobalt hydroxy carbonate.

Experimental

Analytical grade $Co(NO_3)_2 \bullet 6H_2O$, $Na_3PO_4 \bullet 12H_2O$ and urea were used as precursors to prepare the cobalt hydrate carbonate precipitate. 2 mmol of $Co(NO_3)_2 \bullet 6H_2O$ and 19 mg

Na_3PO_4•$12H_2O$ were dissolved in 140 mL deionised water. The solution was kept stirring at the room temperature for 0.5 hour, then 0.6 g urea was added in. After stirred for another 1 hour, the mixture was transferred into an autoclave maintained at 100 ºC for 18 hours. The resultant light purple precipitate was washed with deionised water by filtrating. Dried at 65 ºC for 2 days, half of the product was collected as sample (a), another half of the resultant sample was mixed with 30 mL deionised water, stirred to be suspension. After 4 mL 8 M NaOH solution was added in, the suspension was then treated by adding 4 mL 30% H_2O_2 solution, keeping stirring at room temperature. 0.5 hour later, the mixture was transferred into an autoclave, which was then kept at 45 ºC for 16 hours. Finally, the treated precipitate was washed and dried at 65 ºC for 2 days, collected as sample (b).

Characterisation

X-ray diffraction

X-Ray diffraction patterns were collected using a Philips X'pert wide angle X-Ray diffractometer, operating in step scan mode, with Cu Kα radiation (1.54052 Å).

SEM

The specimens were mounted on SEM mounts with carbon tape and sputter-coated with a thin layer of gold. The scanning electron microscopy (SEM) images were taken with a FEI Quanta 200 operating at 30 kV (FEI Quanta 200 SEM, FEI Company, Hillsboro, Oregon, USA). For X-ray microanalysis (EDX), three samples were embedded in Araldite resin and polished with diamond paste on Lamplan 450 polishing cloth using water as a lubricant. The samples were coated with a thin layer of evaporated carbon for conduction and examined in a JEOL 840A analytical SEM (JEOL Ltd, Tokyo, Japan) at 25kV accelerating voltage. Preliminary analyses of the carbonate mineral samples were carried out on the FEI Quanta SEM using an EDAX X-ray microanalyser, and microanalyses of the clusters of fine crystals were carried out using a full standards quantitative procedure on the JEOL 840 SEM using a JEOL-2300 energy-dispersive X-ray microanalysis system (JEOL Ltd, Tokyo, Japan). Oxygen was not measured directly but was calculated using assumed stoichiometry to the other elements analysed. For the EDX measurements the sample was crushed into tablets and then coated with a thin layer ofevaporated carbon to enhance surface conductivity. After this

preparation, the samples were examined in a JEOL 840A analytical scanning electron microscope (SEM) at a 15 kV accelerating voltage.

XPS

Data was acquired using a Kratos Axis ULTRA X-ray Photoelectron Spectrometer incorporating a 165mm hemispherical electron energy analyser. The incident radiation was Monochromatic Al Kα X-rays (1486.6eV) at 150W (15kV, 10ma) and at 45 degrees to the sample surface. Photoelectron data was collected at take off angle of theta = 90^{o}. Survey (wide) scans were taken at an analyser pass energy of 160eV and multiplex (narrow) high resolution scans of Co 2p, O1s and C1s at pass energy of 20eV. Survey scans were carried out over 1200-0eV binding energy range with 1.0eV steps and a dwell time of 100ms. Narrow high-resolution scans were run with 0.05ev steps and 250ms dwell time. Base pressure in the analysis chamber was $1.0x10^{-9}$ torr and during sample analysis $1.0x10^{-8}$ torr. Atomic concentrations were calculated using the CasaXPS version 2.3.14 software and a linear baseline with Kratos library Relative Sensitivity Factors (RSFs).

A small amount of each finely-powdered sample was carefully applied to double sided adhesive tape on a standard Kratos Axis Ultra sample bar. This was attached to the sample rod of the Load Lock system for initial evacuation to ~ 1 X10-6 torr. The sample bar was then transferred to the UHV Sample Analysis Chamber (SAC) for collection of X-ray Photoemission spectra.

Raman Spectroscopy

Raman spectra were collected using an Olympus BHSM microscope, equipped with 10 and 50×objectives and part of a Renishaw 1000 Raman microscope system, which also includes a monochromator, a filter system and a charge coupled device (CCD). Raman spectra were excited by a HeNe laser (532 nm) at a resolution of 2 cm^{-1} in the range between 100 and 4000 cm^{-1}. Repeated acquisition using the highest magnification was accumulated to improve the signal to noise ratio. Spectra were calibrated using the 520.5 cm^{-1} line of a silicon wafer.

Spectra at elevated temperatures were obtained using a Linkam thermal stage (Scientific Instruments Ltd., Waterford Surrey, England). Spectra were taken from room temperature (25 ºC) at 50 ºC intervals up to a temperature of 550 ºC.

Infrared Spectroscopy

Infrared spectra were obtained using a Nicolet Nexus 870 FTIR spectrometer with a smart endurance single bounce diamond ATR cell. Spectra over the 4000–525 cm^{-1} range were obtained by the co-addition of 64 scans with a resolution of 4 cm^{-1} and a mirror velocity of 0.6329 cm/s. Spectra were co-added to improve the signal to noise ratio.

Spectral manipulation such as baseline adjustment, smoothing and normalisation were performed using the Spectracalc software package GRAMS (Galactic Industries Corporation, NH, USA). Band component analysis was undertaken using the Jandel 'Peakfit' software package which enabled the type of fitting function to be selected and allows specific parameters to be fixed or varied accordingly. Band fitting was done using a Lorentz-Gauss cross-product function with the minimum number of component bands used for the fitting process. The Gauss-Lorentz ratio was maintained at values greater than 0.7 and fitting was undertaken until reproducible results were obtained with squared correlations of r^2 greater than 0.995.

Thermal Analysis

Thermal decomposition of approximately 50mg of hydrotalcite was carried out in a TA® Instruments incorporated high-resolution thermogravimetric analyser (series Q500) in a flowing nitrogen atmosphere (80 cm^3/min), at a rate of 2.0 °C/min up to 1000 °C. For more information on the experimental and analysis techniques used, refer to previous work by the authors [30-35].

Results and Discussion

X-ray diffraction

The X-ray diffraction patterns of the synthesised cobalt hydroxy carbonate together with possible reference patterns are shown in Figure 1. The XRD pattern (a) is that of the synthesised cobalt hydroxy carbonate. The XRD pattern illustrated in (b) is that of the cobalt oxy hydroxide and that in (c) is that of the thermally decomposed product of the cobalt hydroxy carbonate. The compound cobalt hydroxy carbonate has the same formula as many naturally occurring minerals of the rosasite mineral group. The rosasite mineral group is monoclinic or triclinic hydroxy carbonates with the general formula $A_2(CO_3)(OH)_2$ or $AB(CO_3)(OH)_2$ where A and B is cobalt, copper, magnesium, nickel and zinc [36]. In the first formula if A is Co, then we have the synthesised compound produced in this work. In the second formula if A is Co and B is Cu then the compound equivalent to the mineral kolwezite is formed. Minerals in this group include rosasite $[(Cu,Zn)_2(CO_3)(OH)_2]$ [37-39], glaucosphaerite $[(Cu,Ni)_2(CO_3)(OH)_2]$ [40-42], kolwezite $[(Cu,Co)_2(CO_3)(OH)_2]$ [43], mcguinnessite $[(Mg,Cu,)_2(CO_3)(OH)_2]$ [44-47], and nullaginite $[(Ni)_2(CO_3)(OH)_2]$ [48-50]. These minerals are nearly all monoclinic. Our material is orthorhombic. The reference patterns of kolwezite, cobalt oxyhydroxide and cobalt oxide are included in this figure. It is apparent that the XRD patterns of the synthesised cobalt hydroxy carbonate resembles that of the published results for cobalt hydroxy carbonate. The partially decomposed cobalt hydroxy carbonate results in the formation of cobalt oxide (please see the thermal analysis later in this text).

Apart from rosasite the minerals are rare secondary minerals. Besides the chemical composition, the structural relationships between these minerals are demonstrated by the similarity of their powder diffraction patterns [51]. A comparison of the XRD patterns of the synthesised cobalt hydroxy carbonate and kolwezite and two standard cobalt hydroxy carbonate minerals with and without Cu are shown in Figure 1b. The best match of the XRD patterns of the synthesised hydroxy carbonate is with pattern 00-048-0083. This pattern is for a hydrated cobalt hydroxy carbonate.

Scanning Electron Microscopy

The SEM images of the synthesised rosasite type compound are shown in Figure 2. Two types of crystalline habit may be observed. (a) bundles of fibres which seem to be like a bundle of straw tied in the middle and (b) secondly bundles of single crystals radiating out like from a central point. A comparison may be made with the morphology of the rosasite minerals, a significant feature of which is their microcrystalline fibrous habit. This characteristic precludes in most cases, any single crystal studies. Rosasite as with the other minerals of this group form spheroidal aggregates in extremely thin fibrous crystals.

Li et al. Described these morphologies as sisal-like architecture with an average diameter of 15 μm [25]. These authors claimed that this type of architecture is unique. Perhaps for synthetic compounds this is true. However such fibres, nanorods and shapes are very common for many minerals including the rosasite group of minerals. A significant feature of the rosasite minerals is their microcrystalline fibrous habit. This characteristic precludes in most cases, single crystal studies. The space group symmetry and cell parameters are mainly derived from powder pattern indexing. Apart from that of malachite, no other structural determinations are available for the rosasite minerals. Rosasite as with the other minerals of this group form spheroidal aggregates in extremely thin fibrous crystals.

The results of the EDX analyses are as follows:

Element	mass%	At%
C	12.13	24.60
O	34.39	52.35
Si	1.43	1.24
P	0.77	0.61
Co	51.28	21.20

XPS results

The XPS of the synthesised cobalt hydroxy carbonate are displayed in Figure 3 a,b,c. These figures show the binding energy of the cobalt, oxygen and carbon respectively. Three binding energies are observed for Co at 786.0, 782.9 and 781.3 eV. These binding energies may be assigned to the Co-O bonds of the cobalt carbonate unit, the bond between cobalt and water and the bond between cobalt and the OH units. Stoch and Capecki [52] discussed the band shape of the $2p_{3/2}$ bands in the XPS of cobalt compounds as well as Fe and Ni compounds. The broad band on the higher energy side of the main Co peak was described as very broad

'shake-up' bands. These so called 'shake-up' bands make the extraction of important information difficult or impossible. Thus the peaks as shown in Figure 3a may be assigned in different ways and may be interpreted differently. If the binding peak at 786.0 eV is ascribed to the 'shake-up' peak then the band at 782.9 eV is the binding energy of the cobalt bound to carbonate. This value compares well with the bond energy of 782.5 eV reported by Robles-Dutenhefner et al. [53]. Normally the value for the binding energy for cobalt oxides is around 780 to 781 eV. The main peak presented in this work is in this position. This Co binding energy is assigned to the cobalt bound to hydroxyl units. Porta et al. [54] reported the XPS of Co and mixed Co-Cu hydroxy carbonates. The bond energy for the pure Co hydroxy carbonate was found to be 781.2 eV.

The binding energies of oxygen are given in Figure 3b. Three binding energies are found at 533.0, 531.9 and 531.2 eV and are attributed to the binding of the oxygen to water, carbonate and hydroxyl units respectively. Porta et al. [54] reported bond energies for oxygen as 529.6 and 530.4 eV for a Co hydroxy carbonate. These values are slightly less than the values found in this research. The binding energy of carbon shows four binding energies at 289.6, 288.0, 286.4 and 285.0 eV. These binding energies are assigned to the binding energy of carbon in carbonate, C=O, C-O and C-C bonds. These binding energies are associated with the carbon in the carbonate anion. The values determined by Porta et al. were 284.8 eV. These authors did not find any differences in bond energy for the carbon in a Co hydroxy carbonate. The results of the XPS show the compound formed is a hydrated cobalt hydroxy carbonate in harmony with the conclusions from XRD. Stoch and Gablankowska-Kukucz studied the XPS of carbonates formed on oxide surfaces for the O 1s band [55]. These researchers found O 1s values for a cobalt hydroxy carbonate at 530.9, 531.7 and 529.7 eV. The values were attributed to oxide, carbonate and an unknown oxygen. The value of the binding energy of the carbonate in this work of 531.7 eV compares well with the value obtained in this work of 531.89 eV.

Vibrational Spectroscopy

Much understanding of the molecular structure of a material can be readily obtained through the vibrational spectra. The Raman spectra are displayed in a series of figures numbered Figure 4, 7 and 8 which show the Raman spectra in the 800 to 1600 cm^{-1}, 200 to 800 cm^{-1} and 3200 to 3800 cm^{-1} region. The infrared spectra are reported in Figures 5 (500 to

1200 cm^{-1}), Figure 6 (1200 to 1600 cm^{-1}) and Figure 9 (3300 to 3700 cm^{-1}). The Raman spectrum of the cobalt hydroxy carbonate in the 800 to 1600 cm^{-1} region is characterised by an intense sharp peak at 1077 cm^{-1}. This band is assigned to the ν_1 CO_3^{2-} symmetric stretching mode. The shoulder at 1045 cm^{-1} is assigned to a hydroxyl deformation mode. Recently Frost et al. published the vibrational spectra of minerals of the rosasite mineral group [56-59]. The Raman spectrum of spherocobaltite displays a single symmetric band at 1088 cm^{-1}. In the Raman spectrum of kolwezite two comparatively sharp bands are observed at 1093 and 1059 cm^{-1}. In contrast two infrared bands of larger band widths are observed for kolwezite at 1096 and 1047 cm^{-1}. The position of this second band appears to vary between the rosasite minerals. This band attributed to the ν_1 CO_3^{2-} symmetric stretching mode is not observed in the infrared spectrum (Figure 5). Strong infrared bands are observed at 986 and 1048 cm^{-1}. These bands are attributed to OH deformation modes. A low intensity Raman band is found at 996 cm^{-1}. This band is likely to be assigned to a phosphate impurity.

For rosasite, two intense Raman bands are observed at 1096 and 1056 cm^{-1}. In the infrared spectrum two intense bands are observed at 1096 and 1046 cm^{-1} with an additional band at 1023 cm^{-1}. The first band at 1096 cm^{-1} is assigned to the ν_1 symmetric stretching mode of the carbonate unit. Bands have been observed in the infrared spectra of malachite at 1095 cm^{-1} and 1090 cm^{-1} for azurite. The infrared spectrum of hydrocerrusite showed an intense band at 1090 cm^{-1}. Interestingly the $(CO_3)^{2-}$ ν_1 band of the rosasite minerals should not be infrared active. However because of symmetry reduction of the carbonate anion the band becomes activated. The intense Raman band observed at 1096 cm^{-1} for rosasite is assigned to the ν_1 $(CO_3)^{2-}$ symmetric stretching vibration. The intense Raman band at 1056 cm^{-1} is assigned to the δ OH deformation mode. The corresponding infrared band at 1046 cm^{-1} is even of greater intensity. The additional infrared band at 1023 cm^{-1} is also assigned to a δ OH deformation mode. The observation of two δ OH deformation modes is attributed to the non-equivalence of the OH units in the structure.

In the Raman spectrum of the cobalt hydroxy carbonate broad overlapping bands are observed at 1386 and 1467 cm^{-1}. These bands are assigned to the ν_3 CO_3^{2-} antisymmetric stretching mode. Intense infrared bands are observed at 1395, 1466 and 1505 cm^{-1} and are assigned to this vibrational mode. Minor low intensity components are observed at 1597 and 1639 cm^{-1}. These bands are described in terms of water HOH bending modes. For kolwezite two sets of infrared bands are found at (1522 and 1426 cm^{-1}) and (1486 and 1390 cm^{-1}). In

the Raman spectrum of kolwezite in this spectral region, three bands are observed at 1495, 1456 and 1363 cm^{-1}. These bands are assigned to the ν_3 antisymmetric $(CO_3)^{2-}$ stretching modes. The infrared spectrum of rosasite in this spectral region is characterised by intense bands centred upon 1488 and 1388 cm^{-1} which may be resolved into four bands at 1522, 1488, 1425 and 1388 cm^{-1}. In comparison the Raman spectrum displays bands at 1493, 1458 and 1364 cm^{-1}. These bands are attributed to the ν_3 antisymmetric $(CO_3)^{2-}$ stretching modes. In the IR spectrum of malachite two bands are observed at around 1500 and 1400 cm^{-1}. For hydrozincite two bands are observed at 1515 and 1400 cm^{-1}. It would appear that there are two pairs of bands for rosasite namely (1522 and 1425 cm^{-1}) and (1488 and 1388 cm^{-1}). The observation of two sets of bands for rosasite suggests that there are two independent carbonate units in the crystal structure.

An intense sharp infrared band is observed in the infrared spectrum of the synthesised cobalt hydroxy carbonate at 830 cm^{-1} and is assigned to the ν_2 bending modes of the $(CO_3)^{2-}$ units (Figure 5). A second band is observed at 820 cm^{-1} and is also assigned to this vibration. The infrared spectrum of the mineral kolwezite is also similar in this spectral region, even though the profile is more complex. Infrared bands are observed at 878, 861, 819 and 802 cm^{-1}. In comparison only a single Raman band at 818 cm^{-1} is observed. The infrared spectrum of kolwezite displays bands at 747, 728 and 710cm^{-1} corresponding Raman bands are at 751 and 718 cm^{-1}. The mineral rosasite shows two intense infrared bands at 870 and 818 cm^{-1}. These bands are assigned to the ν_2 bending modes of the $(CO_3)^{2-}$ units. The first band is not Raman active as is observed by the absence of any intensity. A Raman band is observed at 817 cm^{-1} which corresponds to the infrared band at 818 cm^{-1}. The observation of two ν_2 bands is in harmony with the observation of two sets of bands in the ν_3 antisymmetric stretching region. The infrared spectrum of malachite shows two bands at 820 and 803 cm^{-1} ascribed to $(CO_3)^{2-}$ ν_2 bending modes as does azurite at 837 and 817 cm^{-1}. Hydrocerrusite infrared spectrum shows two bands at 850 and 834 cm^{-1}.

In the infrared spectrum of the synthesised cobalt hydroxy carbonate, bands are observed at 633, 677 and 741 cm^{-1}. These bands are assigned to the ν_4 $(CO_3)^{2-}$ bending modes. A Raman band is observed at 755 cm^{-1} and is of low intensity. The band is assigned to the ν_4 $(CO_3)^{2-}$ bending mode. The Raman band for cobalticalcite shows a low intensity band at 725 cm^{-1}. Other Raman bands are observed at 445, 521 and 559 cm^{-1}. These bands are attributed to Co-O stretching vibrations. For rosasite a number of infrared bands are

observed at 776, 748 and 710 cm^{-1}. In the Raman spectrum, bands are observed at 751 and 719 cm^{-1}. For malachite two infrared bands are observed at 748 and 710 cm^{-1} which are assigned to this ν_4 $(CO_3)^{2-}$ bending vibration. Another mineral with similar formulation to rosasite, hydrozincite has infrared bands in this region at 738 and 710 cm^{-1}. The infrared spectrum of hydrocerrusite has ν_4 $(CO_3)^{2-}$ bending modes at 700, 687 and 676 cm^{-1}. Two bands are observed around 570 cm^{-1} for rosasite; it is not known if these bands are due to ν_4 $(CO_3)^{2-}$ bending modes.

In the Raman spectrum of the synthesised cobalt hydroxy carbonate, Raman bands are observed at 3507, 3554 and 3615 cm^{-1}. In the infrared spectrum (Figure 9) bands are observed at 3493, 3574 and 3620 cm^{-1}. The first two bands are assigned to water stretching vibrations and the last band to the OH stretching vibration of the hydroxyl units. The observation of water bands provides further evidence that water is involved in the crystal structure of the synthesised compound. The infrared spectrum of kolwezite shows two strong bands at 3400 and 3307 cm^{-1} with corresponding Raman bands at 3389 and 3321 cm^{-1}. Additional infrared bands may be observed at 3541 and 3119 cm^{-1}. The first band is assigned to OH stretching vibrations and the latter band to adsorbed water. The intensity of this band appears to vary with the particular rosasite mineral. The Raman spectrum of rosasite displays two bands at 3387 and 3319 cm^{-1}. In the infrared spectrum four bands are observed at 3486, 3401, 3311 and 3139 cm^{-1}. This latter band not observed in the Raman spectrum is attributed to adsorbed water. The two bands at 3401 and 3311 cm^{-1} appear to correspond to the two Raman bands. These bands are attributed to OH stretching vibrations.

Thermal Analysis

The thermal analysis of the synthetic cobalt hydroxycarbonate is reported in Figure 10. Three mass loss steps are observed at 198, 209 and 808 °C with mass losses of 4.33, 17.5 and 4.2 %. These mass loss steps are attributed to (a) partial dehydroxylation (b) dehydroxylation and decarbonation and (c) loss of phosphate. The theoretical mass loss for the loss of carbonate is 22.75 % and for loss of the OH units is 8.5 %. The total experimental mass loss is 26.03 % which includes a mass loss of 4.2% attributed to the loss of phosphate. This value may be compared with the theoretical mass loss of 31.25%. It is apparent that dehydroxylation and decarbonation take place simultaneously. This result is confirmed by ion current mass spectrometry. In this experiment sodium phosphate was used as a directing

agent. The thermal analysis shows a high temperature peak at above 800°C. This mass loss is attributed to the loss of phosphate. Porta et al. [54] published results of the thermal decomposition of a cobalt hydroxy carbonate and C/Cu hydroxy carbonates with varying Co/Cu ratios. These researchers reported the TG and DTA peaks for the thermal decomposition of a cobalt hydroxy carbonate. They found that the cobalt hydroxy carbonate decomposed in one step at 393K with the processes of dehydroxylation and loss of CO_2. Li et al. also reported the thermal decomposition of cobalt hydroxy carbonate and these authors displayed two thermal analysis patterns of (a) sisal like morphology and (b) rose like morphology. The thermal analysis pattern shown in Figure 8 resembles the first of the patterns described by Li et al. However the thermal analysis patterns of these authors were limited by a temperature of 700 °C and these authors would not observe if any mass losses occurred at higher temperatures over 800 °C.

Conclusions

In an attempt to synthesise nanofibers and nanomaterials of cobalt oxide, a compound cobalt hydroxy carbonate was synthesised and was subsequently characterised by a combination of techniques including X-ray diffraction, SEM, XPS, thermal analysis and vibrational spectroscopy. The formed material showed an XRD pattern similar to that of a hydrated cobalt hydroxy carbonate. The morphology of the synthesised material was fibrous with bundles of fibres on the micron scale. The morphology of the cobalt hydroxy carbonate strongly resembles that of minerals from the rosasite mineral group. These minerals were also found to be fibrous in nature.

Acknowledgements

The financial and infra-structure support of the Queensland University of Technology Inorganic Materials Research Program of the School of Physical and Chemical Sciences are gratefully acknowledged. One of the authors (JY) thanks the Queensland University of Technology for a postgraduate doctoral scholarship.

References

[1] J.H. Fendler, F.C. Meldrum, Adv.Mat. 7 (1995) 607-632.

[2] B.B. Lakshmi, C.J. Patrissi, C.R. Martin, Chem. Mat. 9 (1997) 2544-2550.

[3] Y. Sun, Y. Xia, Nature 298 (2002) 2176-2179.

[4] M.S. Gudiksen, L.J. Lauhon, J. Wang, D.C. Smith, C.M. Lieber, Nature 415 (2002) 617-620.

[5] J.-L. Le Loarer, H. Nussbaum, D. Bortzmeyer, Alumina extrudates, methods for preparing and use as catalysts or catalyst supports. (Rhodia Chimie, Fr.). Application: WO, 1998, p. 44.

[6] V.S. Burkat, V.S. Dudorova, V.S. Smola, T.S. Chagina, Light Metals (Warrendale, PA, United States) (1985) 1443-1448.

[7] C. Nedez, J.-P. Boitiaux, C.J. Cameron, B. Didillon, Langmuir 12 (1996) 3927-3931.

[8] Y. Chen, L. Jin, Y. Xie, Journal of Sol-Gel Science and Technology 13 (1998) 735-738.

[9] D.S. Xue, Y.L. Huang, Y. Ma, P.H. Zhou, Z.P. Niu, F.S. Li, R. Job, W.R. Fahrner, Journal of Materials Science Letters 22 (2003) 1817-1820.

[10] A.P. Philipse, A.-M. Nechifor, C. Patmamanoharan, Langmuir 10 (1994) 4451-4458.

[11] K. Okada, A. Tanaka, S. Hayashi, K. Daimon, N. Otsuka, Journal of Materials Research 9 (1994) 1709-1713.

[12] S. Ananthakumar, V. Raja, K.G.K. Warrier, Materials Letters 43 (2000) 174-179.

[13] J.-M. Chen, C.-T. Hsieh, H.-W. Huang, Y.-H. Huang, H.-H. Lin, M.-H. Liu, S.-C. Liao, H.-C. Shih, Synthesis of composite nanofibers for applications in lithium batteries. (Taiwan). Application: US
US, 2008, pp. 12pp , Cont -in-part of U S Ser No 419,167.

[14] I.-D. Kim, J.-M. Hong, S.-M. Jo, Anode material with nanofiber structure for secondary batteries. (S. Korea). Application: US
US, 2008, p. 23pp.

[15] R.L. Frost, D. Wain, Journal of Thermal Analysis and Calorimetry 91 (2008) 267-274.

[16] T.-L. Lai, Y.-L. Lai, C.-C. Lee, Y.-Y. Shu, C.-B. Wang, Catal. Today 131 (2008) 105-110.

[17] X. Xie, Y. Li, Z.-Q. Liu, M. Haruta, W. Shen, Nature (London, United Kingdom) 458 (2009) 746-749.

[18] Z. Liu, R. Ma, M. Osada, N. Iyi, Y. Ebina, K. Takada, T. Sasaki, J. Am. Chem. Soc. 128 (2006) 4872-4880.

[19] Y. Zhang, Y. Chen, T. Wang, J. Zhou, Y. Zhao, Microporous and Mesoporous Materials 114 (2008) 257-261.

[20] T. Pauporte, L. Mendoza, M. Cassir, M.C. Bernard, J. Chivot, Journal of the Electrochemical Society 152 (2005) C49-C53.

[21] w.-Y. Li, L.-N. Xu, J. Chen, Advanced Functional Materials 15 (2005) 851-857.

[22] B. Geng, F. Zhan, H. Jiang, Z. Xing, C. Fang, Cryst. Growth Des. 8 (2008) 3497-3500.

[23] Y. Shao, J. Sun, L. Gao, The Journal of Physical Chemistry C 113 (2009) 6566-6572.

[24] J.H. Yang, T. Sasaki, Chemistry of Materials 20 (2008) 2049-2056.

[25] B. Li, Y. Xie, C. Wu, Z. Li, J. zhang, Materials Chemistry and Physics 99 (2006) 479-486.

[26] R. Xu, H.C. Zeng, Journal of Physical Chemistry B 107 (2003) 12643-12649.

[27] C. Kaya, J.Y. He, X. Gu, E.G. Butler, Microporous and Mesoporous Materials 54 (2002) 37-49.

[28] D. Kuang, Y. Fang, H. Liu, C. Frommen, D. Fenske, Journal of Materials Chemistry 13 (2003) 660-662.

[29] H.Y. Zhu, G. X. P., D. Y. Song, Y. Q. Bai, S. P. Ringer, Z. Gao, Y. X. Xi, W. Martens, J. D. Riches, R.L. Frost., J. Phys. Chem. B 108 (2004) 4245-4247.

[30] R.L. Frost, M.C. Hales, W.N. Martens, Journal of Thermal Analysis and Calorimetry 95 (2009) 999-1005.

[31] S.J. Palmer, H.J. Spratt, R.L. Frost, Journal of Thermal Analysis and Calorimetry 95 (2009) 123-129.

[32] R.L. Frost, A.J. Locke, M.C. Hales, W.N. Martens, Journal of Thermal Analysis and Calorimetry 94 (2008) 203-208.

[33] V. Vagvoelgyi, L.M. Daniel, C. Pinto, J. Kristof, R.L. Frost, E. Horvath, Journal of Thermal Analysis and Calorimetry 92 (2008) 589-594.

[34] V. Vagvolgyi, R.L. Frost, M. Hales, A. Locke, J. Kristof, E. Horvath, Journal of Thermal Analysis and Calorimetry 92 (2008) 893-897.

[35] V. Vagvolgyi, M. Hales, W. Martens, J. Kristof, E. Horvath, R.L. Frost, Journal of Thermal Analysis and Calorimetry 92 (2008) 911-916.

[36] J.A. Mandarino, Fleischer's Glossary of Mineral Species, The Mineralogical Record Inc., Tuscon, 1999.

[37] D. Lovisato, Atti. accad. Lincei, [2] 17 (1910) 723-728.

[38] G.P. Bolgov, N.A. Rozybakieva, Sbornik Nauch. Trudov Kazakh. Gorno-Met. Inst. (1956) 34-43.

[39] C. Perrier, American Mineralogist 6 (1921) 166.

[40] M.W. Pryce, J. Just, Mineralogical Magazine 39 (1974) 737-743.

[41] L.B. Railsback, Carbonates and Evaporites 14 (1999) 1-20.

[42] J.L. Jambor, Canadian Mineralogist 14, Pt. 4 (1976) 574-576.

[43] M. Deliens, P. Piret, Bulletin de Mineralogie 103 (1980) 179-184.

[44] A.J. Read, Mineralogical Magazine 48 (1984) 457-459.

[45] W. Postl, P. Golob, Mitteilungsblatt - Abteilung fuer Mineralogie am Landesmuseum Joanneum 49 (1981) 293-299.

[46] S. Matsubara, A. Kato, Ganko 88 (1993) 517-524.

[47] R.C. Erd, F.P. Cesbron, F.E. Goff, J.R. Clark, Mineralogical Record 12 (1981) 143-147.

[48] E.H. Nickel, J.A. Hallbert, R. Halligan, Journal of the Geological Society of Australia 26 (1979) 61-71.

[49] E.H. Nickel, L.G. Berry, Canadian Mineralogist 19 (1981) 315-324.

[50] E.H. Nickel, J.F.M. Clout, B.J. Gartrell, Mineralogical Record 25 (1994) 283-291, 302.

[51] F. Zigan, W. Joswig, H.D. Schuster, S.A. Mason, Zeitschrift fuer Kristallographie, Kristallgeometrie, Kristallphysik, Kristallchemie 145 (1977) 412-426.

[52] J. Stoch, A. Capecki, Surface and Interface Analysis 15 (1990) 206-210.

[53] P.A. Robles-Dutenhefner, K.A.d.S. Rocha, E.M.B. sousa, E.V. Gusevskaya, Journal of catalysis 265 (2009) 72-79.

[54] P. Porta, R. Dragone, G. Fierro, M. Inveral, M.L. Jacono, G. Moretti, J. Chem. Soc. Fararday Trans. 88 (1992) 311-319.

[55] J. Stoch, J. Gablankowska-Kukucz, Surface and Interface Analaysis 17 (1991) 165-167.

[56] R.L. Frost, B.J. Reddy, D.L. Wain, W.N. Martens, Spectrochimica Acta, Part A: Molecular and Biomolecular Spectroscopy 66A (2007) 1075-1081.

[57] R.L. Frost, D.L. Wain, W.N. Martens, B.J. Reddy, Spectrochimica Acta, Part A: Molecular and Biomolecular Spectroscopy 66A (2007) 1068-1074.

[58] R.L. Frost, D.L. Wain, W.N. Martens, B.J. Reddy, Polyhedron 26 (2007) 275-283.

[59] R.L. Frost, Journal of Raman Spectroscopy 37 (2006) 910-921.

LIST OF FIGURES

-

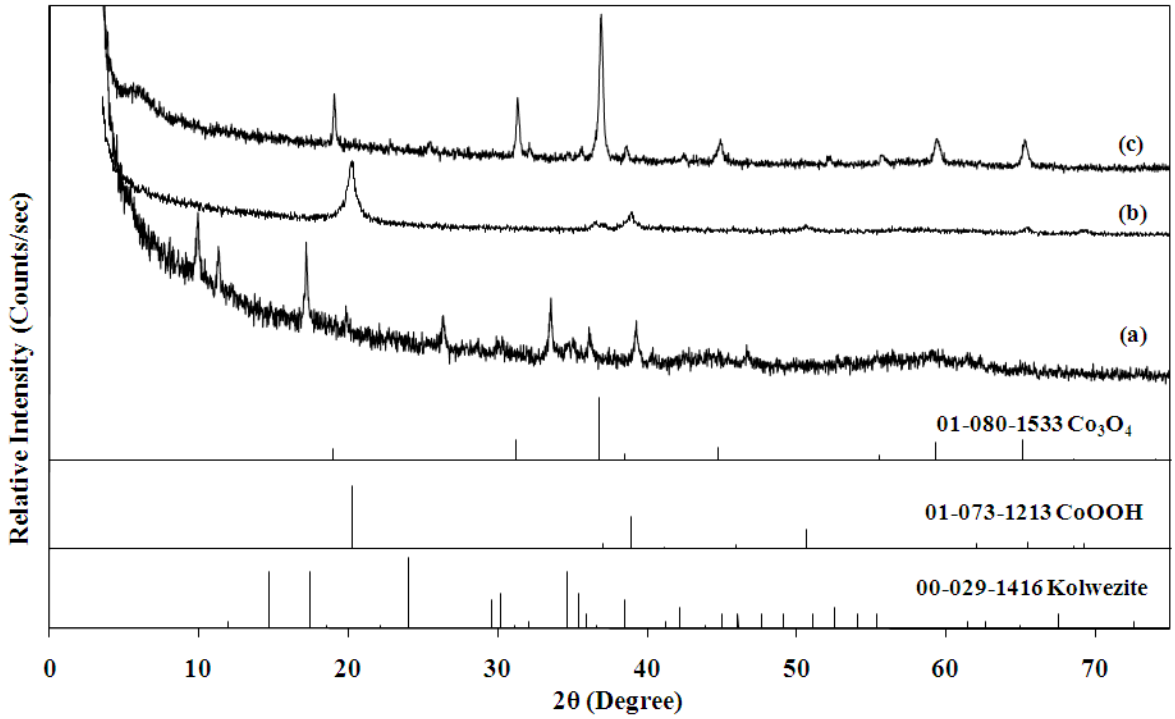

Figure 1a

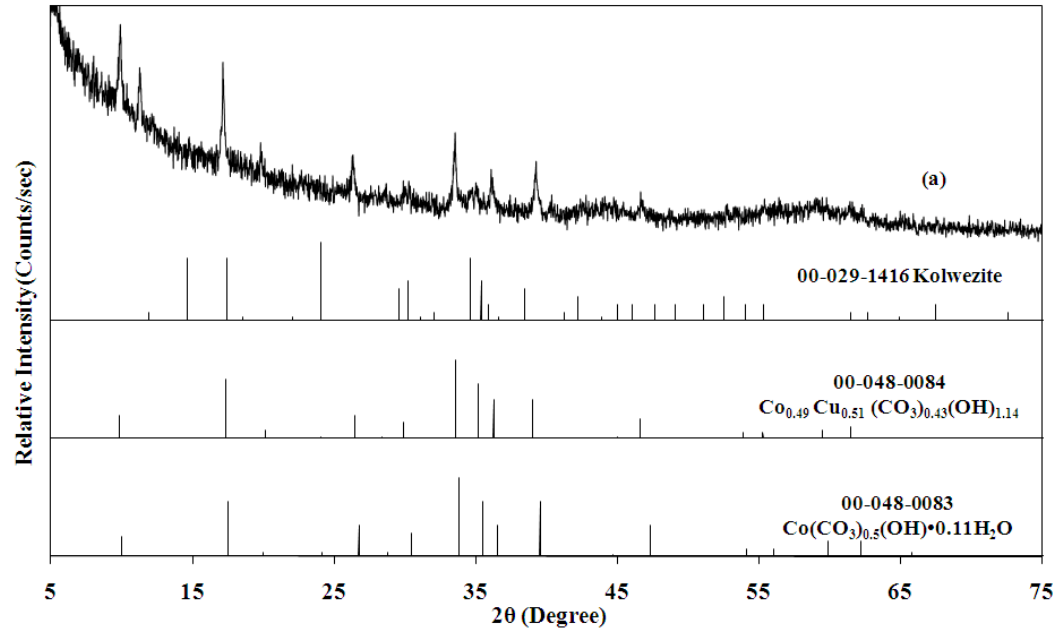

Figure 1b

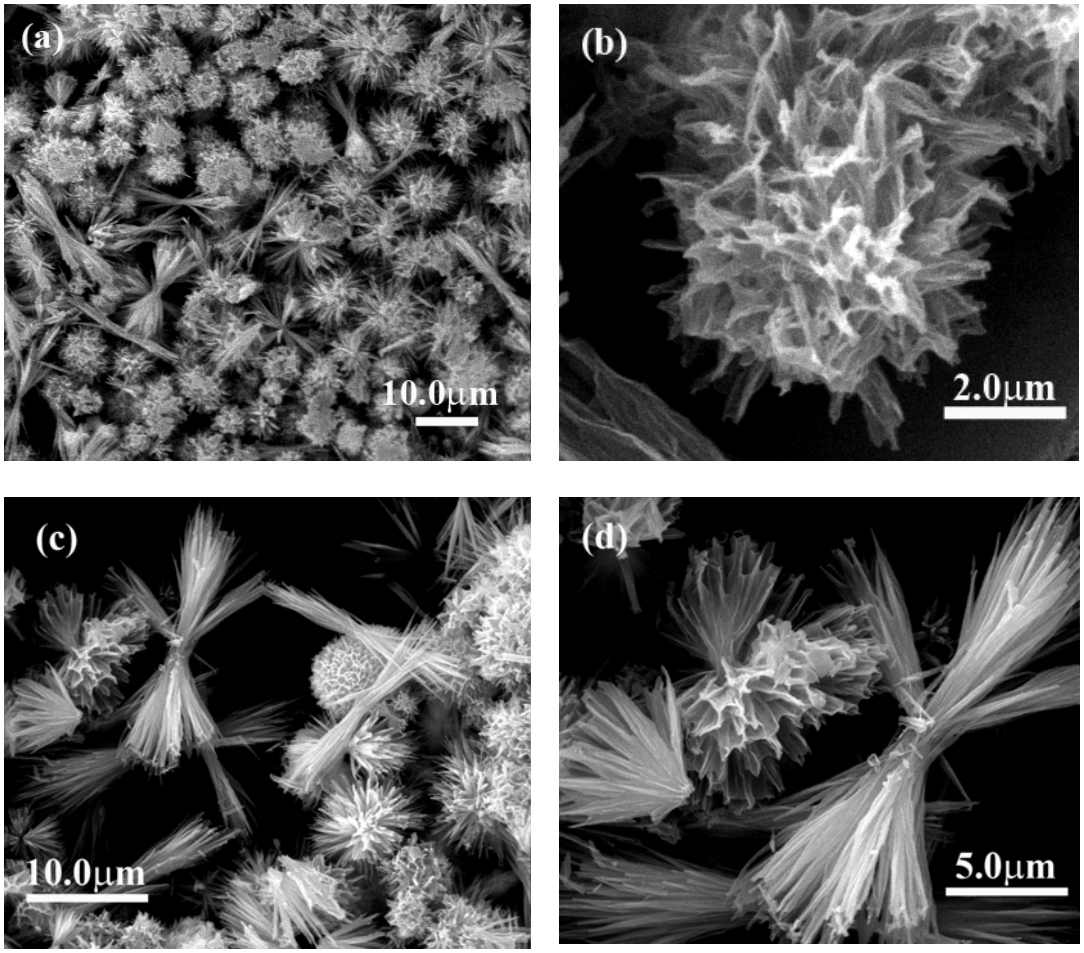

Figure 2

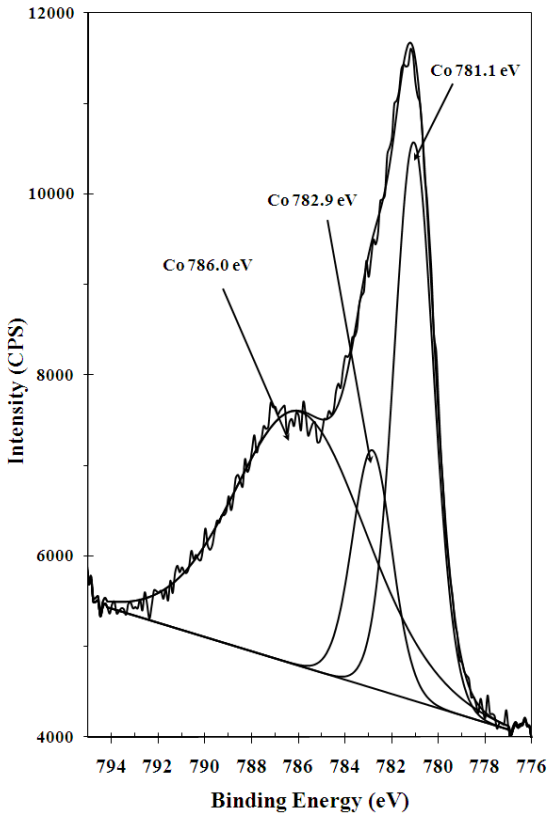
12000
10000
8000
6000
4000
Intensity (CPS)
794 792 790 788 786 784 782 780 778 776
Binding Energy (eV)
Co 781.1 eV
Co 782.9 eV
Co 786.0 eV

Figure 3a

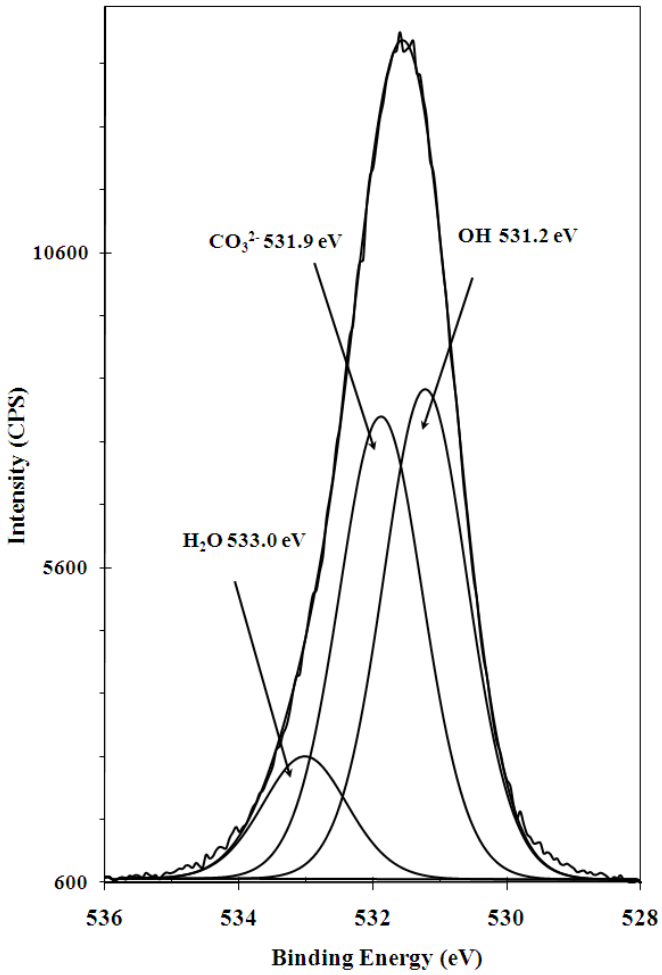
Intensity (CPS)
10600
5600
600
536
534
532
530
528
Binding Energy (eV)
CO3 2- 531.9 eV
OH 531.2 eV
H2O 533.0 eV

Figure 3b

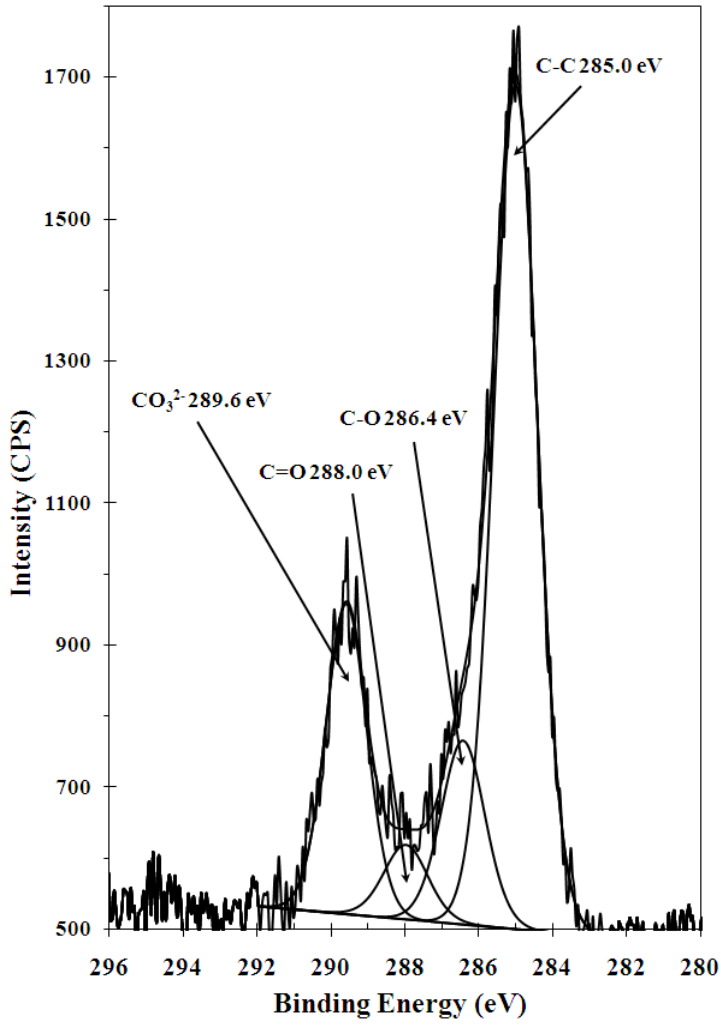
C-C 285.0 eV
C-O 286.4 eV
C=O 288.0 eV
CO3 2- 289.6 eV
Intensity (CPS)
Binding Energy (eV)
1700
1500
1300
1100
900
700
500
296
294
292
290
288
286
284
282
280

Figure 3c

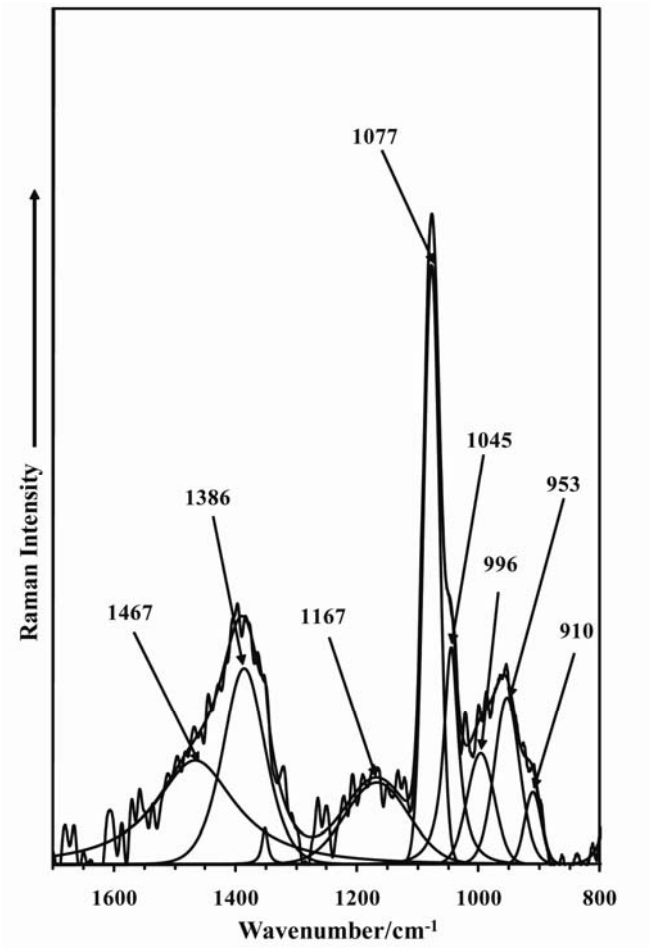
1077
1045
953
1386
996
1467
1167
910
Raman Intensity
1600
1400
1200
1000
800
Wavenumber/cm-1

Figure 4

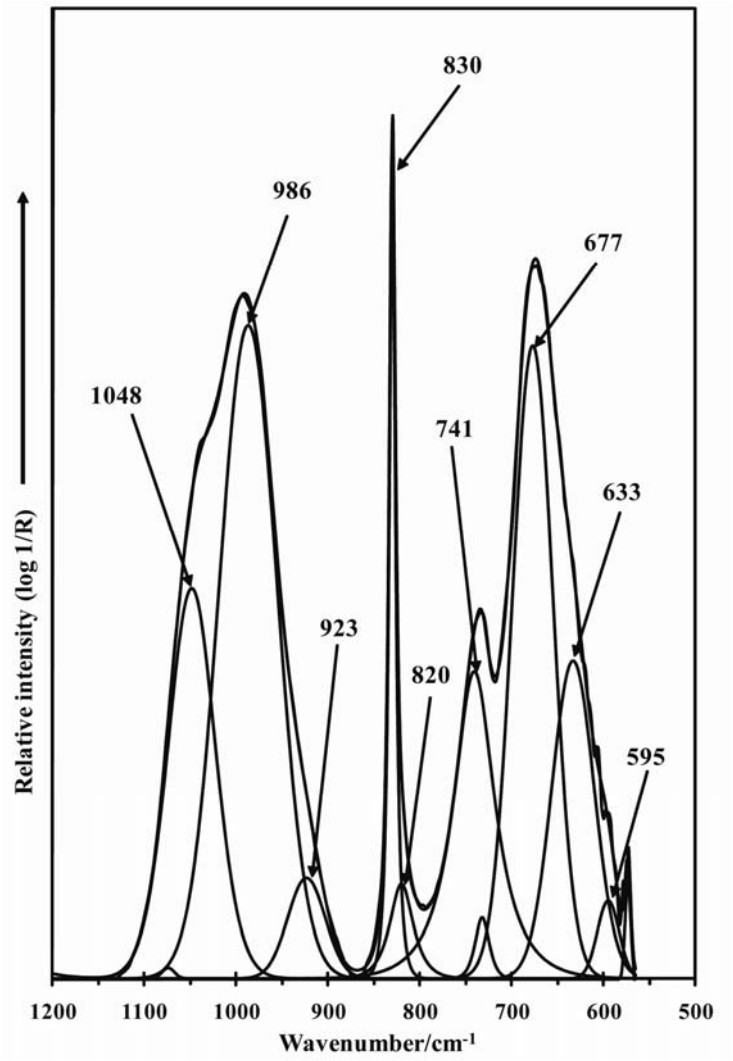
830
986
677
1048
741
633
923
820
595
Relative intensity (log 1/R)
1200
1100
1000
900
800
700
600
500
Wavenumber/cm-1

Figure 5

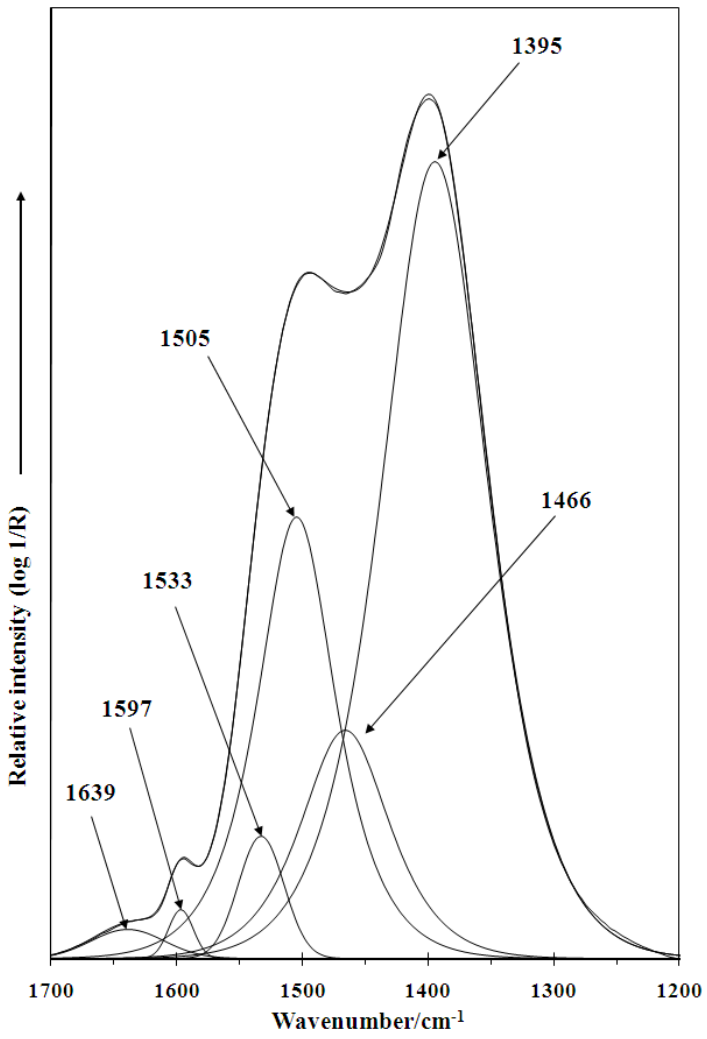
1395
1505
1466
1533
1597
1639
Relative intensity (log 1/R)
1700
1600
1500
1400
1300
1200
Wavenumber/cm-1

Figure 6

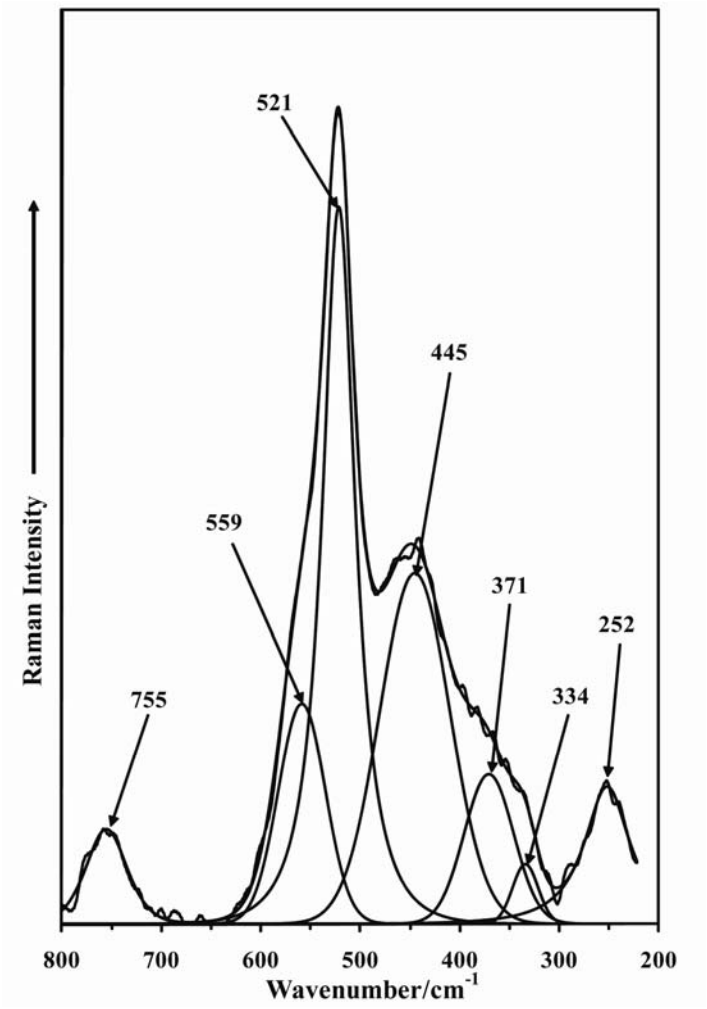
521
445
559
371
252
334
755
Raman Intensity
800
700
600
500
400
300
200
Wavenumber/cm-1

Figure 7

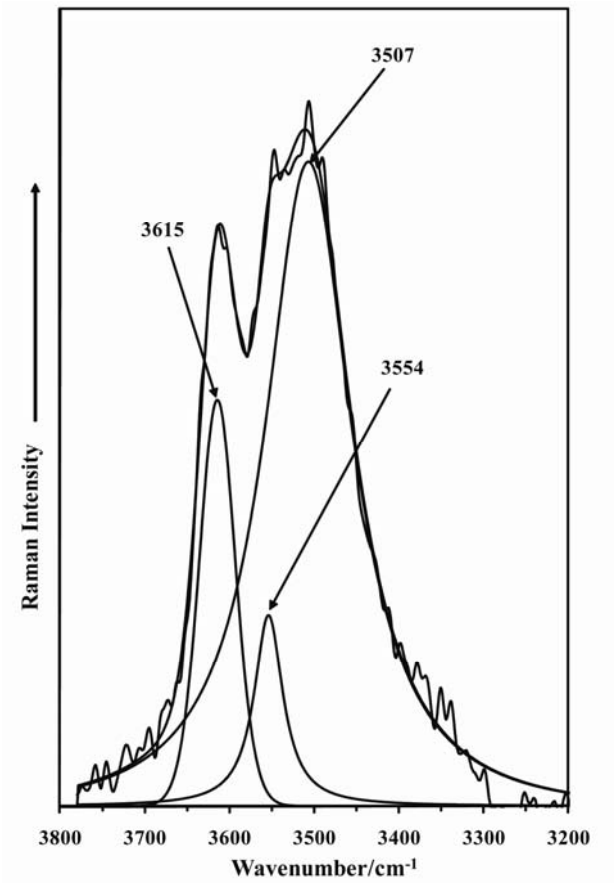
3507
3615
3554
Raman Intensity
3800
3700
3600
3500
3400
3300
3200
Wavenumber/cm-1

Figure 8

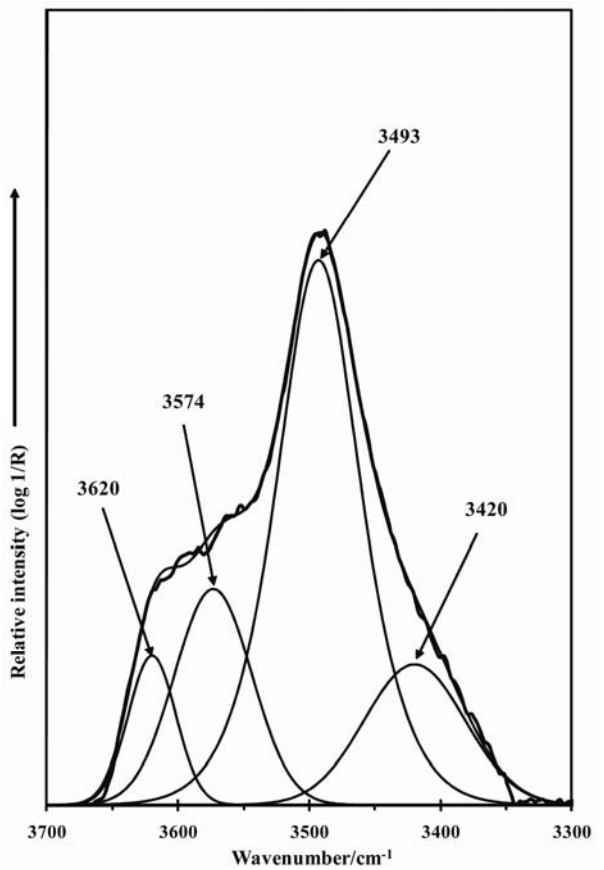
3493
3574
3620
3420
Relative intensity (log 1/R)
3700
3600
3500
3400
3300
Wavenumber/cm-1

Figure 9

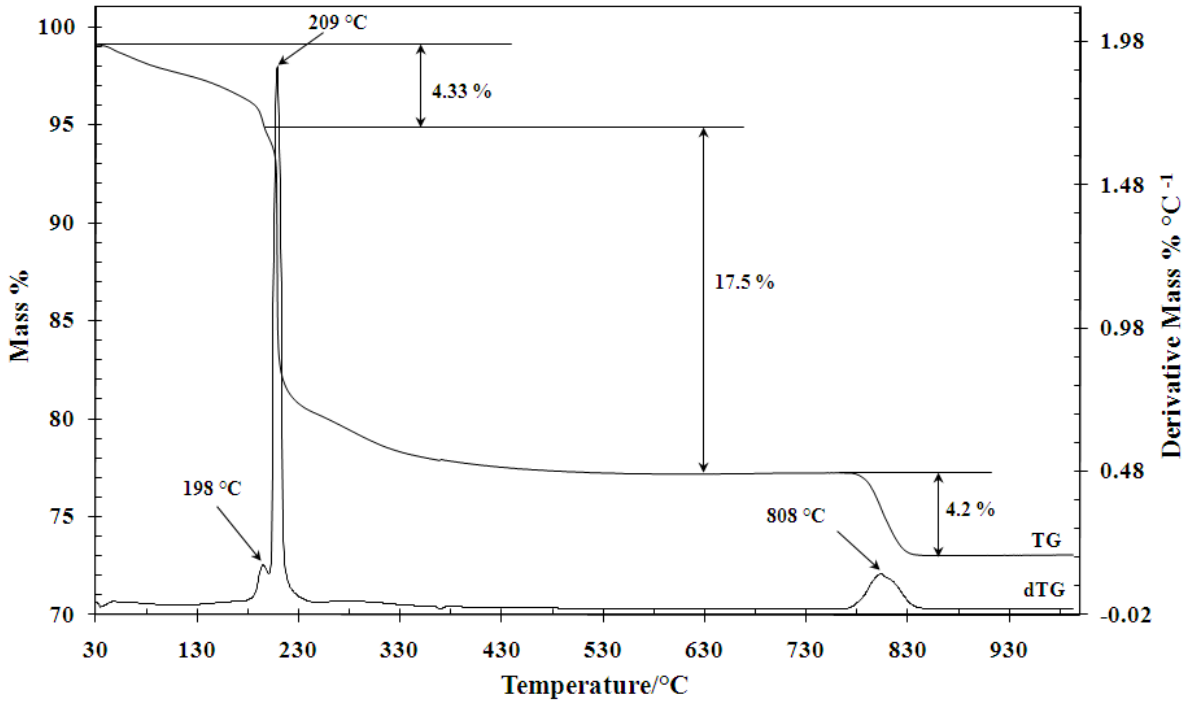
209 °C
4.33 %
17.5 %
198 °C
808 °C
4.2 %
TG
dTG
Mass %
Derivative Mass % °C -1
Temperature/°C
100
95
90
85
80
75
70
1.98
1.48
0.98
0.48
-0.02
30
130
230
330
430
530
630
730
830
930

Figure 10